Dynamic Instabilities and Mechanism of the Electrochemical Oxidation of Thiosulfate

Zhanhe Du,[†] Qingyu Gao,*[,†] Jiamin Feng,[†] Yongchao Lu,[†] and Jichang Wang*[,‡]

College of Chemical Engineering, China University of Mining and Technology, Xuzhou, Jiangsu Province, 221008, PRC, and Department of Chemistry and Biochemistry, University of Windsor, 401 Sunset Avenue, Windsor, Ontario, Canada N9P 3P4

Received: July 9, 2006; In Final Form: August 25, 2006

The electrochemical oxidation of thiosulfate is revealed to have two distinct oscillatory regimes in both linear potential and galvanic voltammograms, where various nonlinear behaviors such as period-2, mixed-mode and quasi-periodic oscillations, and chaos are observed under potentiostatic or galvanostatic conditions. Electrochemical impedance spectroscopy and *iR* compensation characterization indicate that, depending on the operating conditions, the system could be either a strictly potentiostatic oscillator or an S-shaped negative differential resistance oscillator. Chronoamperometry measurements reveal that the first oscillatory process involves a single-electron transfer, whereas within the second oscillatory regime the average number of electrons transferred is around 3.8. Measurements with capillary electrophoresis and chemical methods illustrate that the oxidation products include $S_2O_6^{2-}$, $S_4O_6^{2-}$, $S_5O_6^{2-}$, $S_3O_6^{2-}$, and SO_4^{2-}.

1. Introduction

Thiosulfate represents one of the most promising less-toxic alternatives to cyanide for the leaching and recovery of precious metals.[1,2] As a conventional fixing reagent, thiosulfate has been extensively used in the photoindustry for more than two centuries.[3] From biological aspects, thiosulfate as well as polythionates are commonly used as energy sources for photoautotrophic or chemolithotrophic microorganisms,[4] or they could be employed as a detoxification agent against acrylonitrile-induced neurotoxicological effects by replenishing glutathione.[5] Due to the existence of multiple oxidation states of sulfur, thiosulfate is also an interesting reactant in the study of macroscopic reaction dynamics. Indeed, ever since the report of the first sulfur-compounds-containing chemical oscillator by Epstein et al. in 1982,[6] oxidations of sulfur-containing species have garnered increasing attention.[7−25]

Various nonlinear phenomena have been reported in the oxidation of thiosulfate, such as bistability, birhythmicity, periodic and aperiodic complex oscillations, and temperature compensation behavior in a continuous-flow stirred tank reactor (CSTR).[6,14−19] In addition, pH oscillations have also been observed in the oxidation of thiosulfate in a CSTR or in a semibatch reactor.[20−24] When coupled with diffusion transportations, traveling waves were achieved in the hydrogen peroxide−thiosulfate−sulfite medium.[25] The capability of exhibiting such rich dynamical behavior has made the oxidation of sulfur compounds an attractive model system for the understanding of nonlinear chemical kinetics. Despite the fact that a large amount of effort has been dedicated to the study of sulfur-containing chemical oscillators, the chemical resources of the observed nonlinear instabilities remain to be understood. Earlier studies have suggested that oxidants may have played an essential role in causing chemical oscillations in sulfur-based oscillators;[26] however, recent studies, in particular the observation of pH oscillations in oxidations of sulfur compounds, imply that sulfur chemistry could be responsible for oscillations in those sulfur-based chemical oscillators.[20−24]

Motivated by our recent success in obtaining oscillations in the electrochemical oxidation of sulfide and thiourea,[8,11] in this work we investigated the electrochemical oxidation of thiosulfate with an attempt to gain insights into (1) the oxidation properties of thiosulfate and (2) the role of sulfur reactions in the oscillatory dynamics. As shown in the following, two distinct oscillatory regimes were obtained in the electrochemical oxidation of thiosulfate under both potentiostatic and galvanostatic conditions. Further investigation illustrates that, depending on the applied potential or current density, this new electrochemical oscillator could be a strictly potentiostatic oscillator or an S-shaped negative differential resistance (S-NDR) oscillator,[27−29] implying that the variety of oxidation states of sulfur played a critical role in the nonlinear instabilities.

2. Experimental Procedures

A single cylindrical cell with an internal diameter of 5.5 cm and volume of 40 mL was used in this study. The working electrode was a polycrystalline platinum disk with a diameter of 2.0 mm (CH Instruments Inc.), and the counter electrode was a Pt wire. A Hg/Hg_2SO_4 electrode filled with saturated K_2SO_4 solution or a saturated calomel electrode (SCE) was applied as the reference electrode. The three electrodes formed an equilateral triangle with a distance of 1.8 cm. All potentials reported in this study were versus the Hg/Hg_2SO_4 electrode. Before each experiment, the working electrode was first polished with fine alumina powder (0.05 μm) and was then immersed in a mixture of HNO_3 (60%) and H_2O_2 (30%) with a volume ratio of 1:1 at 60.0 °C for 30.0 min. After that, cyclic potential sweeps between −0.65 and 0.8 V at a scan rate of 1.0 V/s were performed in 0.5 M H_2SO_4 solution for 30.0 min to further clean the electrode surface. Thereafter, the Pt electrode was rinsed repeatedly with Milli-Q water and was transferred into the test solution under the protection of a water droplet on its surface.

* Corresponding authors. Tel/Fax: +86 516 399 5758 (Gao); Tel: +1 519 253 3000 ext 3540, Fax: +1 519 973 7098 (Wang). E-mail: gaoqy@cumt.edu.cn (Gao), jwang@uwindsor.ca (Wang).
[†] China University of Mining and Technology.
[‡] University of Windsor.

10.1021/jp064312l CCC: $33.50
Published on Web 12/06/2006

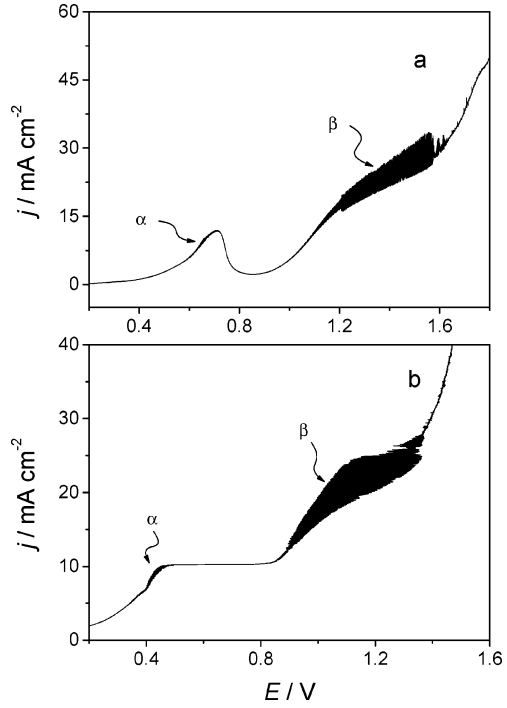

Figure 1. (a) Linear voltammogram of 0.50 M thiosulfate at a scan rate of 0.01 mV/s, and (b) linear galvanic voltammogram obtained at a scan rate of 0.01 mA/s.

The temperature of the reaction cell was kept constant through a circulating water bath (Polyscience Instruments) at 20.0 ± 0.1 °C except as otherwise stated.

All electrochemical oxidation experiments were performed on a CHI-660A electrochemical workstation (CH Instruments Inc.). The electrochemical impedance spectroscopy (EIS) was measured with an IM6e electrochemical workstation (Zahner-eletrik Gmbh Co. KG). The capillary electrophoresis (CE) analysis was performed on a P/ACE MDQ (Beckman) equipped with a diode array detector (DAD). A fused-silica capillary of 57.0 cm (50.0 cm to the detector) × 75-μm i.d. × 375-μm o.d. was used. The sample was injected into the capillary by an overpressure. A negative voltage of 30 kV was applied for separation, and 195.0 nm was selected for the spectrophotometric detection.

Water used in all experiments was purified through a Millipore Milli-Q system (18.2 MΩ cm). All reagents used were analytical grade. Before each experiment, oxygen was removed from the solution by bubbling with ultrapure nitrogen gas. The electrolyte solution contained 0.5 M thiosulfate unless otherwise stated. Under the above reaction conditions, the resistance between the working and reference electrodes was 34 ± 2 Ω, which was determined from the impedance measurements at a high frequency (10 kHz).

3. Nonlinear Instabilities

Figure 1a presents a linear potential voltammogram of 0.5 M thiosulfate solution at a scan rate of 0.01 mV/s, in which two distinct oscillatory regimes denoted by α and β are observed in this quasi-stationary study. The first oscillatory window, α, occurs when the external potential is between 0.55 and 0.70 V. The second oscillatory window, β, is much wider (1.0−1.6 V) in comparison with the first one, and the amplitude of oscillations within the window β is significantly larger than that of oscillations in the window α. Notably, in Figure 1a, there is a branch of negative slope between about 0.7 and 0.8 V. The observed decay in the current density might be simply caused by the depletion of thiosulfate as the above $i-E$ measurement was conducted on a stationary electrode without stirring.[30] However, our analysis indicates that at such a low scan rate as used in Figure 1a, the thickness of the Nernst diffusion layer would be increased to about 0.5 cm when the potential sweeps from 0.7 to 0.8 V. Considering that the diffusion layer would be destroyed by convections caused by density gradients or vibration, a thickness of 0.5 cm cannot be reached in practice. Therefore, we conclude that a negative $i-E$ branch is intrinsic in this studied system. This conclusion is further supported by measurements of $i-E$ curves with a rotating disk electrode to eliminate the depletion effect or with an ultramicroelectrode, where negative differential resistances are still obtained. According to existing theories,[27−29] nonlinear instabilities shall also be observable within the potential region between 0.7 and 0.8 V.

The linear galvanic voltammogram in Figure 1b also exhibits two oscillatory regimes: α between 4.5 and 11.0 mA/cm^2 and β between 11.5 and 30 mA/cm^2. The distance between the two oscillatory windows in Figure 1b is rather small. It is consistent with the result in Figure 1a in which oscillations in the potential windows α and β overlap around the current density 10.0 mA/cm^2. In general, the two oscillatory regimes in Figure 1, parts a and b, are related to each other and should be considered as the same oscillatory window achieved under different operating modes, that is, potentiostatic or galvanostatic.

Figure 2 presents four time series of current densities achieved in the oscillation window α (see Figure 1). In Figure 2a, only simple oscillations of one peak per period are observed under a static potential of 0.52 V. Gradually decreasing the potential from 0.52 V caused a smooth decrease in the amplitude of oscillations and eventually drove the system to a stable steady state. Such a scenario implies that a supercritical Hopf-bifurcation takes place here. Figure 2, parts b and c, shows mixed-mode oscillations (MMOs) at 0.56 and 0.62 V. Although a small peak in Figure 2b appears at the bottom of the large-amplitude oscillations, MMOs in Figure 2, parts b and c, can be denoted as 1^2-type MMOs , where the superscript indicates the number of small-amplitude peaks within each cycle.[31] If the potential increases still, the system returns to simple periodic oscillations as shown in Figure 2d. No oscillatory behavior was observed when the applied potential was increased to above 0.7 V.

Typical oscillations in the current density within the parameter window β are shown in Figure 3. When the external potential was equal to 1.0 V, only simple oscillations were obtained (see Figure 3a). As the potential was increased to 1.1 V in Figure 3b, 1^1-type MMOs were observed. Oscillations in Figure 3b are somehow slightly irregular. In Figure 3c, the potential was increased to 1.4 V, where each oscillation cycle contained two large peaks and there was a shoulder on each large peak. If the potential was increased still further (see Figure 3d), simple oscillations were restored. The transition from simple to complex and then from complex to simple oscillations is similar to the one seen in Figure 2.

Nonlinear instabilities under galvanostatic conditions are characterized in Figure 4, where oscillations in the potential are examined within the oscillation window α in Figure 1b. Shown in Figure 4a are simple periodic oscillations at the current density of 4.77 mA/cm^2. When the current density was increased to 5.09 mA/cm^2, 1^1-type MMOs appeared in Figure 4b. Further increase of the current density resulted in the appearance of 1^2-type MMOs in Figure 4c. Besides different oscillatory

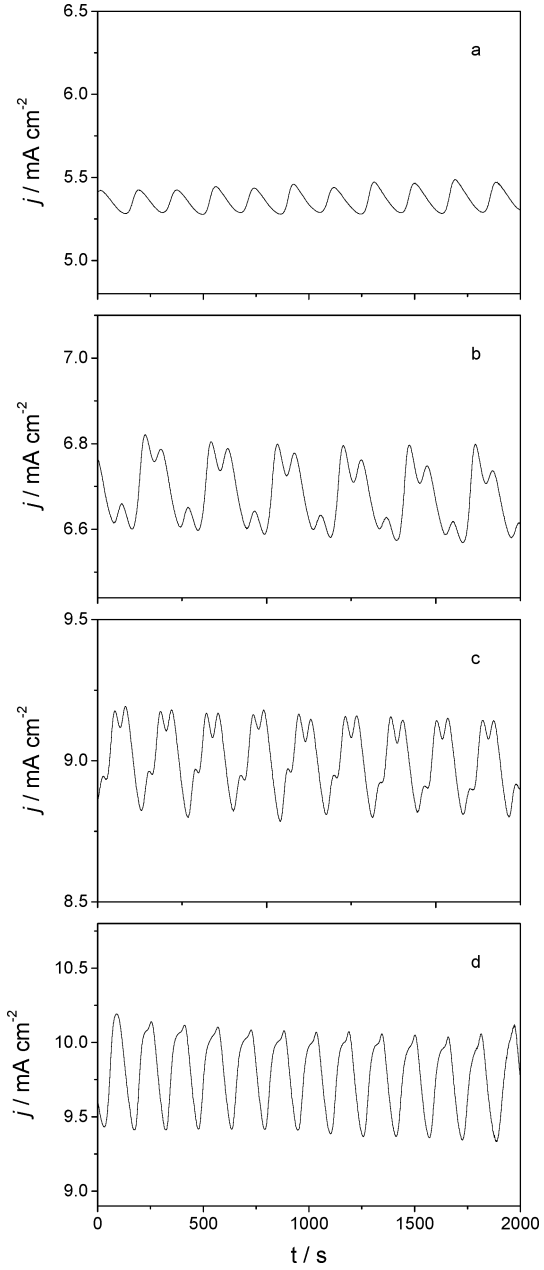

Figure 2. Time series of current density conducted at different static potentials: (a) 0.52 V, (b) 0.56 V, (c) 0.62 V, and (d) 0.64 V. The electrolyte solution contains 0.50 M thiosulfate.

phenomena, Figure 4 also demonstrates that the average potential of the thiosulfate system increases as the current density is increased.

Figure 5 displays five time-series obtained within the parameter window β of Figure 1b. Small-amplitude oscillations developed as the applied current density was increased to above 11.5 mA/cm^2. The smooth increase in the oscillation amplitude implies that the electrochemical oxidation of thiosulfate undergoes a supercritical Hopf-bifurcation here. An example of simple oscillations is plotted in Figure 5a, in which the current density was equal to 17.51 mA/cm^2. As the current density was increased, quasi-periodic oscillations were obtained (see Figure 5b). Further increase of the current density resulted in the occurrence of irregular behavior in Figure 5c, although the waveform of these irregular oscillations still possesses the character of quasi-periodic oscillations. Calculations of the power spectrum and the largest Lyapunov exponent (0.004) suggest that these irregular oscillations are chaotic.[32] If the

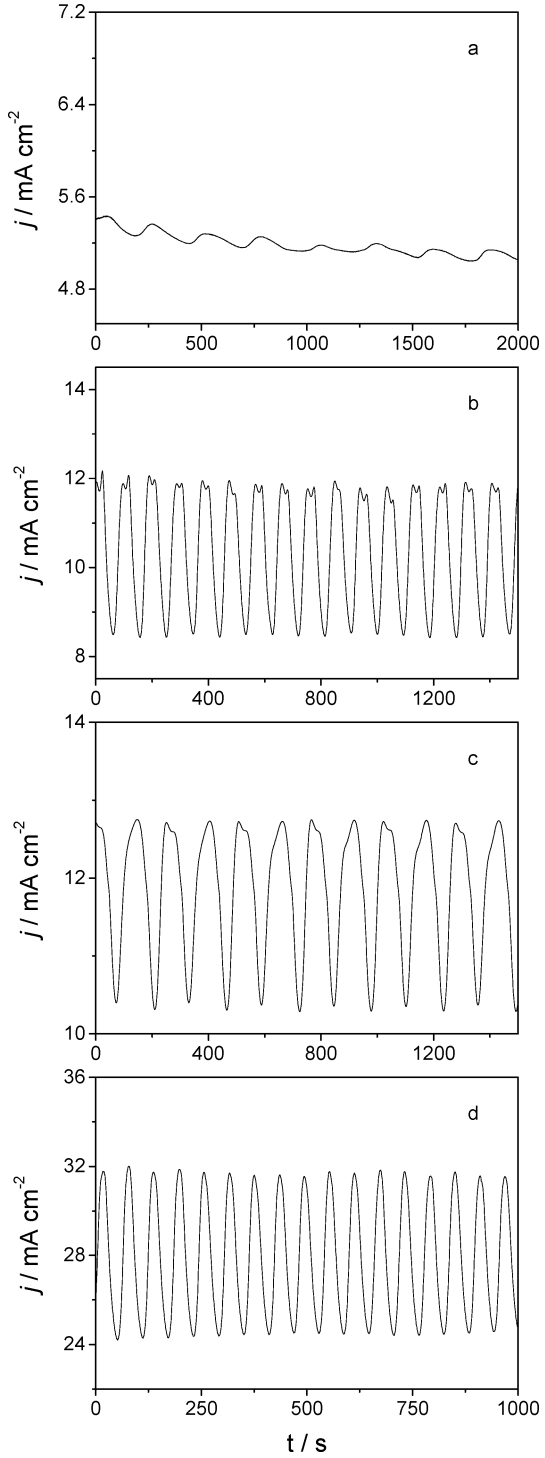

Figure 3. Time series of current density conducted at different potentials: (a) 1.0 V, (b) 1.1 V, (c) 1.4 V, and (d) 1.5 V. The electrolyte solution contains 0.50 M thiosulfate.

current density was increased continuously, a reverse period-doubling bifurcation took place, leading the system back to simple periodic oscillations (from Figure 5d to 5e).

When the *iR* compensation technique was applied under the potential control condition, oscillations within the oscillation window α disappeared. Such a scene suggests that the double-layer potential Φ_{DL} plays an essential role in the above observed nonlinear instabilities.[27] In contrast, oscillations within the oscillatory window β persisted even under the vanishing ohmic resistance, implying that oscillations within the parameter window β are better classified as a strictly potentiostatic

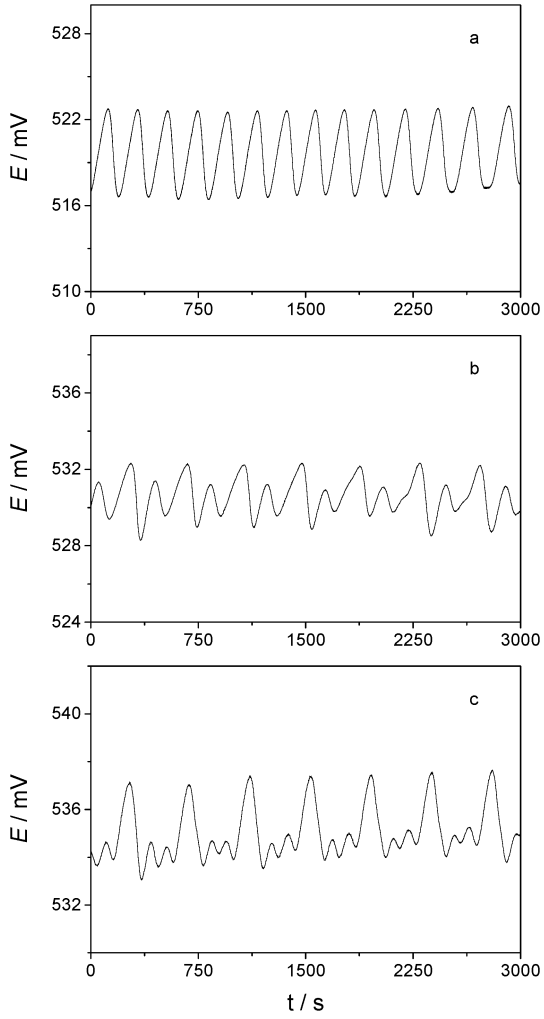

Figure 4. Time series of potential performed under different current densities: (a) 4.77 mA/cm^2, (b) 5.09 mA/cm^2, and (c) 5.73 mA/cm^2. The electrolyte solution contains 0.50 M thiosulfate.

oscillator, in which both the positive and negative feedback loops are purely chemical.

Oscillations within the window α have been obtained under both potentiostatic (Figure 2) and galvanostatic (Figure 4) conditions, and these oscillations appear around a branch of positive slope in the linear voltammograms, exhibiting features of a hidden N-shaped negative differential resistance oscillator (HN-NDR).[27−29] Interestingly, the electrochemical impedance spectroscopy (EIS) conducted within the potential range between 0.2 and 1.6 V shows a semicircular arc with a linear region at the low-frequency limit (see Figure 6), greatly different from the EIS of a HN-NDR oscillator, which is expected to display negative real impedance within a range of moderate perturbation frequency and positive impedance at the low frequency.[27−29] EIS in Figure 6 suggests that the oxidation process is indeed controlled by the charge transfer and mass transportations.[30] When the *iR* potential drop of the solution is subtracted from the potential used in Figure 1a, an S-shaped voltammogram appears around 0.55 V and the current density oscillates around the internal branch of the S-shaped plot. It suggests that oscillations within the window α is a Class II, S-NDR oscillator, in which the double-layer potential is a negative feedback variable.

Except within a narrow potential range between 0.65 and 0.75 V, the radius of the semicircle in the above EIS measurements is found to decrease with the increase of the potential,

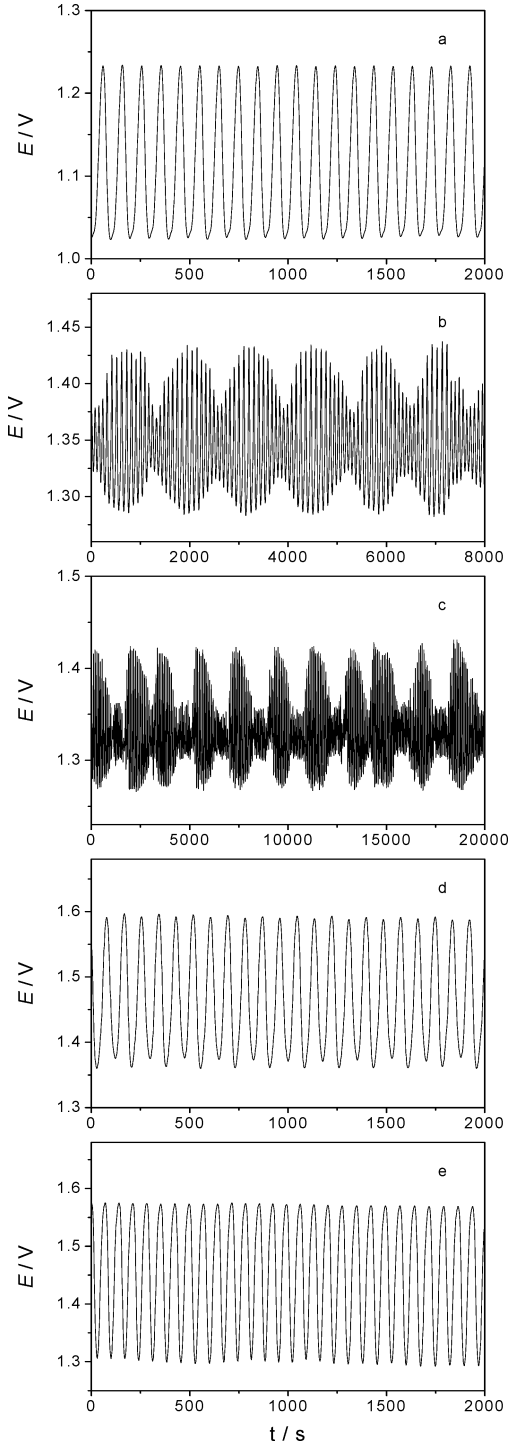

Figure 5. Time series of potential performed under different current densities: (a) 17.51 mA/cm^2, (b) 23.24 mA/cm^2, (c) 24.19 mA/cm^2, (d) 25.78 mA/cm^2, and (d) 29.28 mA/cm^2. The electrolyte solution contains 0.50 M thiosulfate.

implying that charge-transfer resistance (R_{ct}) increases with the potential. Accordingly, a negative differential resistance (NDR) is expected within this potential range if the increment of the charge-transfer overpotential (η_{ct}) is not as significant as R_{ct}. To evaluate the contribution of R_{ct} to the current flowing through the cell, Figure 7 plots the dependence of $1/R_{ct}$ on the applied potential, in which R_{ct} is measured from EIS in the potential range from 0.2 to 1.4 V with a step size of 0.05 V. The plot in Figure 7 possesses the same characteristics as the $i-E$ curve in Figure 1a, indicating that effects of the applied potential on η_{ct} are not significant. In Figure 7, there is also a branch with a

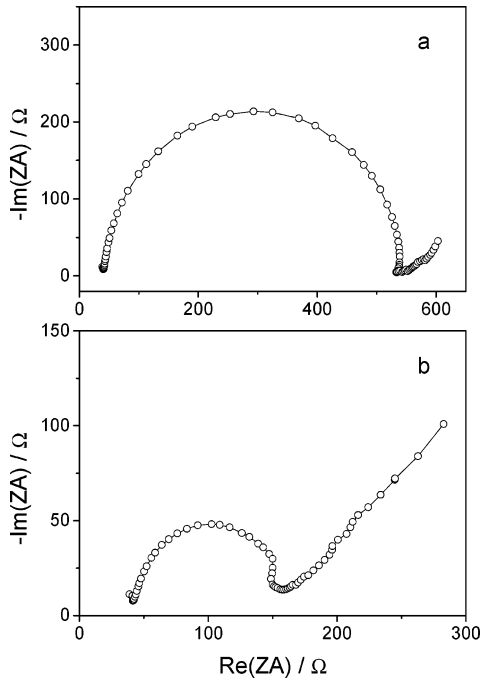

Figure 6. Electrochemical impedance spectroscopy measured at different potentials: (a) 0.55 V, and (b) 1.2 V. The external excitation frequency is decreased from 100.0 kHz to 10.0 mHz, and the amplitude of modulation potential is 10.0 mV.

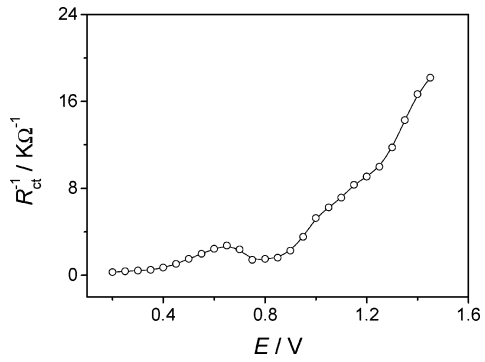

Figure 7. The influence of potential on the inverse charge-transfer resistance.

negative slope within the potential range between 0.65 and 0.80 V, which is consistent with the NDR region achieved in Figure 1a. Although the majority of reported electrochemical oscillations are related to the NDR in the $i-E$ curve, surprisingly no oscillatory phenomenon is observed within such a potential range in this system, even after external resistances are employed.

4. Mechanistic Characterization

Cyclic voltammetry, chronoamperometry, capillary electrophoresis, and a titration method were employed in the following to decipher the chemical processes occurring in each oscillatory regime. Figure 8a shows the cyclic voltammograms obtained in the absence (dash line) and presence (solid line) of 20.0 mM thiosulfate in a supporting electrolyte (0.25 M sodium perchlorate) solution. For the supporting electrolyte solution, adsorptions and discharge of H_2O occur when the potential is above 0.65 V and the evolution of oxygen takes place when the potential exceeds about 1.2 V. In the negative sweep, a cathodic peak arises at about -0.08 V and is attributed to the reduction of the adsorbed oxide monolayer. After 20.0 mM thiosulfate is

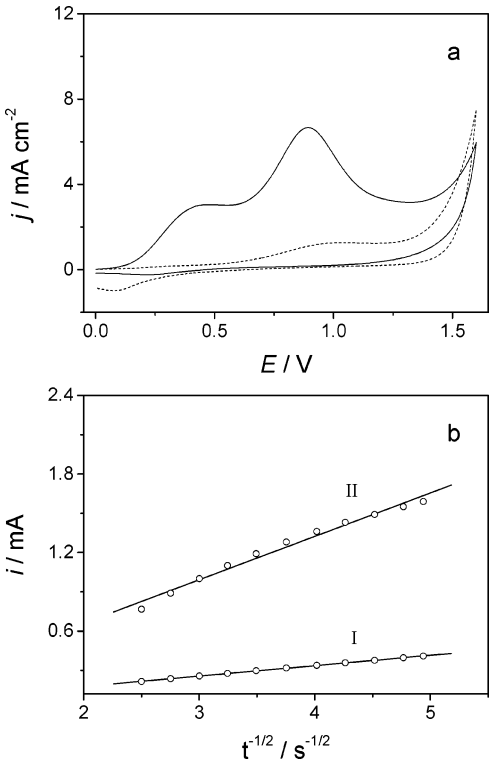

Figure 8. (a) Cyclic voltammogram in the absence (dash line) and presence (solid line) of 20.0 mM thiosulfate at a scan rate of 0.1 V/s. (b) The plot of i vs $t^{-1/2}$ from chronoamperometry, in which the initial potential is -0.6 V and the step potential is 0.5 V (I) and 1.0 V (II), respectively. Other conditions are the following: $[S_2O_3^{2-}] = 20.0$ mM, $[ClO_4^-] = 0.25$ M, and $T = 25.0 \pm 0.1$ °C.

added to the solution, two anodic peaks are obtained. The first oxidation process commences when the potential is above about 0.1 V. When the potential exceeds 0.6 V, further oxidations occur. The potential is somehow lower than that seen in Figure 1a. It may be attributed to influences of resistance and temperature. The second oxidation process occurs within the potential window of H_2O discharge and thus might be an oxygen-transfer reaction, in which the discharge of H_2O plays an important role.

Chronoamperometry was conducted with a solution consisting of 0.25 M $NaClO_4$ and 20.0 mM $Na_2S_2O_3$ to determine the number of electrons transferred at each process. For each measurement, the initial potential was set to -0.6 V at which no faradic process occurred. The potential was then stepped to 0.5 or 1.0 V at which the faradic current was controlled by diffusion transportations. The response of current to the potential step is described by the Cottrell equation:

$$i(t) = \frac{nFAD^{1/2}C^*}{\pi^{1/2}t^{1/2}} \quad (1)$$

where D and C^* are the diffusion coefficient and bulk concentration of $Na_2S_2O_3$, respectively, n is the number of electrons transferred during the process, and A is the area of the electrode surface. The plot of i vs $t^{-1/2}$ is shown in Figure 8b, in which the value of n is achieved from the slope. Parameter values used in Figure 8b are $D = 0.67 \times 10^{-5}$ cm^2/s,[33] $C^* = 20.0$ mM, and $A = 3.14 \times 10^{-2}$ cm^2. At 0.5 V, the result is $n = 0.9 \pm 0.1$ equiv mol^{-1}, that is consistent with early studies which suggest that thiosulfate is mainly oxidized to tetrathionate under such a potential value.[34,35] However, n is only 3.8 ± 0.1 equiv mol^{-1} at the potential $E = 1.0$ V. This suggests that,

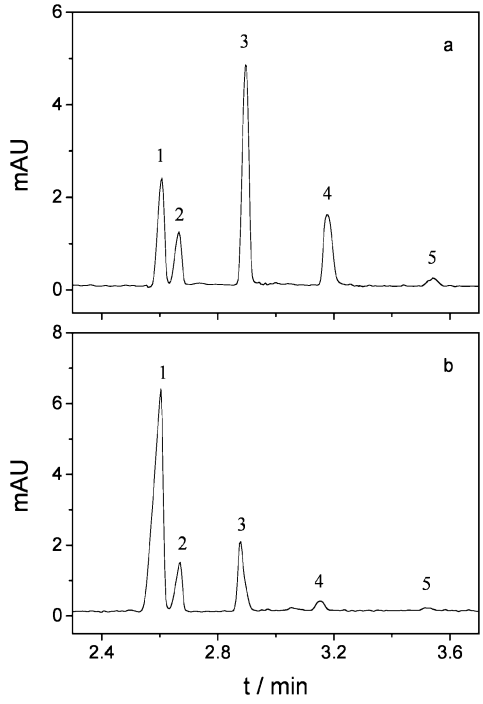

Figure 9. Electropherograms of the electrolysis products conducted at different potentials: (a) 0.5 V, and (b) 1.0 V. Initial compositions of the solution are the following: $[S_2O_3^{2-}] = 20.0$ mM, and $[ClO_4^-] = 0.25$ M. The reaction temperature is 25.0 ± 0.1 °C. Peaks on the electropherogram represent the following: 1, $S_2O_3^{2-}$; 2, $S_2O_6^{2-}$; 3, $S_3O_6^{2-}$; 4, $S_4O_6^{2-}$; and 5, $S_5O_6^{2-}$. The flow solvent contains 5.0 mM KH_2PO_4 and 5.0 mM $(NH_4)_2SO_4$. The sample was diluted 50 times before analysis.

besides sulfate, other products are also formed during the second oxidation process, since *n* would be equal to 8.0 equiv mol^{-1} if thiosulfate is exclusively oxidized to sulfate.

To determine compositions of the oxidation products, potentiostatic electrolysis of 0.25 M $KClO_4$ solution containing 20.0 mM $Na_2S_2O_3$ is performed for over 48 h under magnetic stirring. To avoid the influence of SO_4^{2-} leaking from the reference electrode, a SCE was used, but all the potentials reported here were converted to versus Hg/Hg_2SO_4. Figure 9a presents the electropherogram obtained for the electrochemical oxidation at 0.5 V. As can be seen in Figure 9, besides the residual $S_2O_3^{2-}$, major oxidation products include $S_4O_6^{2-}$, which agrees with the earlier chronoamperometry measurement. In addition, the electropherogram demonstrates that $S_3O_6^{2-}$ and $S_5O_6^{2-}$ are also formed at this potential. In Figure 9b, $S_4O_6^{2-}$, $S_2O_6^{2-}$, $S_3O_6^{2-}$, and $S_5O_6^{2-}$ are obtained in the electrochemical oxidation of thiosulfate at 1.0 V. Direct observation also shows that the element sulfur is produced at 1.0 V, but not at 0.5 V. After allowing the electrolysis at 1.0 V to proceed for 1 week, SO_4^{2-} is detected by titration. We would like to point out that earlier studies have speculated the production of $S_2O_6^{2-}$ during the electrochemical oxidation of thiosulfate;[34] our CE measurements presented in Figure 9 provide the first concrete experimental support for that.

For reactions within the oscillation window α, the number of electrons transferred was determined to be 0.9 ± 0.1 equiv mol^{-1} and $S_4O_6^{2-}$, $S_5O_6^{2-}$, $S_2O_6^{2-}$, and $S_3O_6^{2-}$were detected by CE. According to existing literature,[35,36] the following reactions are proposed:

$$S_2O_3^{2-} \rightarrow S_2O_3^{-\bullet} + e^- \quad \text{(R1)}$$

$$2S_2O_3^{-\bullet} \rightarrow S_4O_6^{2-} \quad \text{(R2)}$$

$$S_4O_6^{2-} + S_2O_3^{2-} \rightarrow S_5O_6^{2-} + SO_3^{2-} \quad \text{(R3)}$$

$$2SO_3^{2-} \rightarrow S_2O_6^{2-} + 2e^- \quad \text{(R4)}$$

$$S_4O_6^{2-} + SO_3^{2-} \rightarrow S_2O_3^{2-} + S_3O_6^{2-} \quad \text{(R5)}$$

Resembling the bulk oxidation oscillation of CO on the Pt,[29] the adsorption of $S_2O_3^{2-}$ and its removal from the electrode surface through reactions R1−R3 could be responsible for oscillatory instability. Further characterizations along this aspect will be pursued in the future.

Within the potential window *β*, SO_4^{2-} is formed by the complete oxidation of $S_2O_3^{2-}$, which can be summarized as[34]

$$S_2O_3^{2-} + 5H_2O \rightarrow 2SO_4^{2-} + 8H^+ + 8e^- \quad \text{(R6)}$$

As demonstrated in cyclic voltammetries (Figure 8) and early studies,[37,38] the oxidation of thiosulfate under these potentials is a typical oxygen-transfer reaction, in which the anodic discharge of H_2O (R7) plays an important role.

$$H_2O \rightarrow OH\bullet_{ads} + H^+ + e^- \quad \text{(R7)}$$

$S_2O_3^{2-}$ is oxidized indirectly through a chemical reaction with the adsorbed hydroxyl radicals, $OH\cdot_{ads}$. As suggested by Brevett and Johnson,[38] $HOS_2O_3^-$ is the most possible intermediate. Such a process can be described as

$$S_2O_3^{2-} + 2OH\bullet_{ads} \rightarrow HOS_2O_3^- + OH^- \quad \text{(R8)}$$

$HOS_2O_3^-$ can react with $S_2O_3^{2-}$ (R9)[18,19,22] or be further oxidized to $S_2O_6^{2-}$ and SO_4^{2-} by $OH\bullet_{ads}$ (R10,11):[38]

$$S_2O_3^{2-} + HOS_2O_3^- \rightarrow S_4O_6^{2-} + OH^- \quad \text{(R9)}$$

$$HOS_2O_3^- + 4OH\bullet_{ads} \rightarrow S_2O_6^{2-} + H^+ + 2H_2O \quad \text{(R10)}$$

$$HOS_2O_3^- + 6OH\bullet_{ads} \rightarrow 2SO_4^{2-} + 3H^+ + 2H_2O \quad \text{(R11)}$$

Similar to reactions between $S_4O_6^{2-}$ and H_2O_2 in homogeneous solution,[22] the following reaction is expected:

$$S_4O_6^{2-} + 2OH\bullet_{ads} \rightarrow 2HOS_2O_3^- \quad \text{(R12)}$$

Thus, a positive feedback is built up by (R9 + R12)

$$S_2O_3^{2-} + HOS_2O_3^- + 2OH\bullet_{ads} \rightarrow 2HOS_2O_3^- + OH^- \text{(R9 + R12)}$$

or through 2R9 + R12

$$S_4O_6^{2-} + 2S_2O_3^{2-} + 2OH\bullet_{ads} \rightarrow 2S_4O_6^{2-} + 2OH^- \text{(2R9 + R12)}$$

As reactions R3, R5, R10, and R11 consume $HOS_2O_3^-$ or $S_4O_6^{2-}$ from the autocatalytic cycle, they serve as negative feedbacks.

5. Conclusions

Nonlinear instabilities are observed in the electrochemical oxidation of thiosulfate on a polycrystalline platinum electrode. The system has two distinct oscillatory regimes, in which various

oscillations such as period-doubled, mixed-mode, and quasi-periodic oscillations and chaos are uncovered. The first oscillatory window which exists within the potential range between 0.5 and 0.7 V under potentiostatic conditions or in the current range between 4.5 and 11.0 mA/ cm^2 under galvanostatic conditions can be classified as an S-NDR oscillator, in which the autocatalysis process is implemented by chemical processes with the double-layer potential Φ_{DL} being a negative feedback variable. The second oscillatory window which exists between 1.0 and 1.6 V under a potentiostatic mode and between 11.5 and 30 mA/cm^2 under a galvanostatic condition persists even in the absence of any potential drop in solution and the external circuit. Therefore, the second oscillatory window is likely a strictly potentiostatic oscillator, in which both the positive and negative feedbacks are pure chemical.[27,28]

The existence of such rich oscillatory phenomena demonstrates that thiosulfate is an attractive reagent for the study of nonequilibrium behaviors in electrochemical reactions. As the chemical process plays a critical role in the instabilities during the electrochemical oxidation of thiosulfate, results obtained here may provide useful information for the understanding of sulfur-containing chemicals oscillators.

Acknowledgment. This work is supported through NSFC (20573134), RFDP (20050290512), and NCET (05-0477) of China. J.W. thanks NSERC for financial support and CUMT for a visiting professorship.

Supporting Information Available: Power spectrum of the time series shown in Figure 5c and attractors obtained by delay methods. This material is available free of charge via the Internet at http:// pubs.acs.org.

References and Notes

(1) Aylmore, M. G.; Muir, D. M. *Miner. Eng.* **2001**, *14*, 135.
(2) Grosse, A. C.; Dicinoski, G. W.; Shaw, M. J.; Haddad, P. R. *Hydrometallurgy* **2003**, *69*, 1.
(3) Adani, K. G.; Barley, R. W.; Pascoe, R. D. *Miner. Eng.* **2005**, *18*, 1269.
(4) Faou, A. L.; Rajagopal, B. S.; Daniels, L.; Fauque, G. *FEMS Microbiol. Lett.* **1990**, *75*, 351.
(5) Enongene, E. N.; Sun, P. N.; Mehta, C. S. *Environ. Toxicol. Pharmacol.* **2000**, *8*, 153.
(6) Orbán, M.; Kepper, P. De; Epstein, I. R. *J. Phys. Chem.* **1982**, *86*, 431.
(7) Chen, A.; Miller, B. *J. Phys. Chem. B* **2004**, *108*, 2245.
(8) Feng, J.; Gao, Q.; Xu, L.; Wang, J. *Electrochem. Commun.* **2005**, *7*, 1471.
(9) Orbán, M.; Epstein, I. R. *J. Am. Chem. Soc.* **1985**, *107*, 2302.
(10) Rábai, G.; Orbán, M.; Epstein, I. R. *J. Phys. Chem.* **1992**, *96*, 5414.
(11) Xu, L.; Gao, Q.; Feng, J.; Wang, J. *Chem. Phys. Lett.* **2004**, *397*, 265.
(12) Rábai, G.; Beck, M. T. *J. Chem. Soc., Dalton Trans.* **1985**, 1669.
(13) Doona, C. J.; Blittersdorf, R.; Schneider, F. W. *J. Phys. Chem.* **1993**, *97*, 7258.
(14) Maselko, J.; Epstein, I. R. *J. Phys. Chem.* **1984**, *88*, 5305.
(15) Orbán, M.; Epstein, I. R. *J. Am. Chem. Soc.* **1987**, *109*, 101.
(16) Orbán, M.; Epstein, I. R. *J. Phys. Chem.* **1982**, *86*, 3907.
(17) Maselko, J.; Epstein, I. R. *J. Chem. Phys.* **1984**, *80*, 3175.
(18) Kovács, K. M.; Rábai, G. *Phys. Chem. Chem. Phys.* **2002**, *4*, 5265.
(19) Rábai, G.; Hanazaki, I. *Chem. Commun.* **1999**, 1965.
(20) Orbán, M.; Epstein, I. R. *J. Phys. Chem.* **1995**, *99*, 2358.
(21) Rábai, G.; Beck, M. T. *J. Phys. Chem.* **1988**, *92*, 2804.
(22) Rábai, G.; Hanazaki, I. *J. Phys. Chem. A* **1999**, *103*, 7268.
(23) Strizhak, P. E.; Pojman, J. A. *Chaos* **1996**, *6*, 461.
(24) Rábai, G; Epstein, I. R. *J. Am. Chem. Soc.* **1992**, *114*, 1529.
(25) Gao, Q.; An, Y.; Wang, J. *Phys. Chem. Chem. Phys.* **2004**, *6*, 5389.
(26) Rábai, G.; Orbán, M. *J. Phys. Chem.* **1993**, *97*, 5935.
(27) Strasser, P.; Eiswirth, M.; Koper, M. T. M. *J. Electroanal. Chem.* **1999**, *478*, 50.
(28) Krischer, K. In *Modern Aspects of Electrochemistry*; Conway, B. E., Bockris, J. O'M., White, R. E., Eds.; Kluwer Academic/Plenum: New York, 1999; Vol. 32, p 1.
(29) Krischer, K. In *Advances in Electrochemical Science and Engineering*; Alkire, R. C., Kolb, D. M., Eds.; Wiley-VCH: New York, 2003; Vol. 8, p 89.
(30) Bard, A. J.; Faulkner, L. R. *Electrochemical Methods: Fundamentals and Application*, 2nd ed.; Wiley: New York, 2001.
(31) Hudson, J. L.; Mankin, J. C. *J. Chem. Phys.* **1981**, *74*, 6171.
(32) Wolf, A; Swift, J. B.; Swinney, H. L.; Vastano, J. A. *Physica D* **1985**, *16*, 285.
(33) Pournaghi-Azar, M. H.; Razmi-Nerbin, H. *Electroanalysis* **2001**, *13*, 465.
(34) Feng, J.; Johnson, D. C. *J. Electrochem. Soc.* **1995**, *142*, 2618.
(35) Tasaka, A.; Takchashi, O.; Migamonto, M. *Denki Kagaku* **1979**, *47*, 608.
(36) Foss, O.; Taniguchi, K. *Acta Chem. Scand.* **1961**, *15*, 1607.
(37) Edwards, J. O. *Chem. Rev.* **1952**, *50*, 455.
(38) Brevett, C. A. S.; Johnson, D. C. *J. Electrochem. Soc.* **1992**, *139*, 1314.